
AN HVS-ORIENTED SALIENCY MAP PREDICTION MODEL

Qiang Li

Image and Signal Processing Lab
University of Valencia
Valencia, 46980, Spain

qiang.li@uv.es

March 25, 2022

ABSTRACT

Visual attention is one of the most significant characteristics for selecting and understanding the outside redundancy world. The nature complex scenes, including larger redundancy and human vision, cannot be processing all information simultaneously because of the information bottleneck. The human visual system mainly focuses on dominant parts of the scenes to reduce the input visual redundancy information. It is commonly known as visual attention prediction or visual saliency map. This paper proposes a new saliency prediction architecture WECSF which inspired by human low-level visual cortex function. The model consists of opponent color channels, wavelet transform, wavelet energy map, and contrast sensitivity function for extracting low-level image features and maximum approximation to the human visual system. The proposed model is evaluated several datasets, including MIT1003¹, MIT300², TORONTO³, SID4VAM⁴ and UCF Sports dataset⁵ to explain its efficiency. The proposed model results are quantitatively and qualitatively compared to other state-of-the-art saliency prediction models. Compared with the baseline model, our model achieved very good performance. Secondly, we also confirmed Fourier/Spectral inspired saliency prediction models has the best prediction scores compared to other start-of-the-art non-neural network and even deep neural network models on the simple image features saliency prediction. Finally, the model also can be applied to spatial-temporal saliency prediction and got better performance.

Keywords visual saliency · redundancy · low-level visual cortex · opponent color channel · wavelet energy map · contrast sensitivity function

1 Introduction

Visual attention or selection is a significant perception function in the Human Vision System (HSV) to drive compact information from the complex nature scenes [Treisman and Gelade, 1980]. The nature scene images, including amount redundancy and usually useless for scene categories or recognition. Visual attention mechanism can extract essential features from redundant data, which benefit visual information processing efficiency in the brain. The phenomenon of visual attention has been studied for a long time [Sun and Fisher, 2003]. Based on Barlow's *Efficiency Coding Hypothesis*, visual attention can be used to explain Barlow's theory. It has used to select relevant information and remove irrelevant information from redundant vision scenes [Barlow, 1959]. Vision saliency has already become a hot research topic spanning neuroscience and computer vision disciplines. In general, there are two types of visual

¹<http://people.csail.mit.edu/tjudd/WherePeopleLook/index.html>

²<http://saliency.mit.edu/>

³<http://www-sop.inria.fr/members/Neil.Bruce/>

⁴http://www.cvc.uab.es/neurobit/?page_id=53

⁵https://www.crcv.ucf.edu/data/UCF_Sports_Action.php

attention mechanisms: bottom-up and top-down branches. Bottom-up models are mainly stimulus-driven. They are used to extract image features accompanied by visual information processing in the brain, e.g., color, frequency, texture, orientation, and motion [Wang et al., 2005]. In contrast, the top-down approach, which is goal-driven, is usually high-level cognitive feedback and modulates low-level vision functional at a specific level [Itti, 2000]. In summary, both above computational neural modeling has been achieved application successfully in the saliency map prediction.

Many studies have tried to estimate bottom-up or top-down computational modeling to predict the saliency map. One of the earliest classical computational modelings was based on bottom-up mechanisms proposed by Itti *et al.* [Itti et al., 1998]. The model estimates the saliency map based on a human low-level vision system, mainly extracting low-level image features, e.g., color, orientation, and intensity conspicuity map. The model structure can be defined by linear filtering (colors, intensity, orientations), center-surround differences and normalization, across-scale combinations and normalization, linear combinations. The model achieved a good result in the saliency prediction. Recently, wavelet transform (WT) has also begun to estimate the computational vision saliency map [Murray et al., 2011]. Compared to the Fourier Transform, it has a high resolution in both the frequency- and the time-domain. WT can decompose signals on different scales is also known as multi-resolution/multi-scale analysis or called sub-band coding that captures more low-level features from the original signal [Louis et al., 1997]. On the other hand, The WT approach can explain the primary visual cortex (V1) properties and produced multi-scale and multi-orientation features when given stimulus. The final saliency map estimate sums up all the processed wavelet coefficients then inverse WT (IWT) [Selvaraj and Shebiah, 2009]. The shortcomings of WT estimate saliency map loss of global contract information rather than local contrast information. However, wavelet energy (WE) maps have barely been considered in the saliency map estimation. Therefore, we implemented WE into the proposed computational modeling.

Furthermore, in the last few years, some studies have tried to estimate the saliency map with deep convolutions neural networks (CNNs). They have achieved impressive performances compared to conventional methods [Borji, 2019, Kruthiventi et al., 2016]. Compared to conventional methods, deep learning implantation easier to transfer to real-life applications, such as object detection, video understanding, and image compression.

In this study, we proposed a low-level human vision cortex inspired saliency prediction framework. The model introduces the opponent color channels, wavelet energy map, and Contrast Sensitivity Function (CSF) to predict human visual attention. The proposed model is stimuli-driven model or bottom-up model and it evaluate with certain metrics, e.g. Area under ROC curve (AUC) [Borji et al., 2013], Normalized Scanpath Saliency (NSS) [Emami and Hoberock, 2013], Pearson’s Correlation Coefficient (CC) [Engelke et al., 2012], Similarity or Histogram Intersection (SIM) [Riche et al., 2013], Kullback-Leibler divergence (KL) [Wilming et al., 2011], and Information Gain (IG) [Kümmerer et al., 2015b]. The details of the above metrics will introduce in section 3. The proposed model was quantitatively evaluated with MIT1003, TORONTO and SID4VAM datasets compared with other different models.

Model	Authors	Year	Inspiration
ITII	[Itti et al., 1998]	1998	Biological
Achanta	[Achanta et al., 2009]	2009	Fourier/Spectral
AIM	[Bruce and Tsotsos, 2005]	2005	Biological/Information-Theoretic
HFT	[li et al., 2012]	2013	Fourier/Spectral
ICL	[Hou and Zhang, 2008]	2008	Information-Theoretic
SIM	[Murray et al., 2011]	2011	Biological
BMS	[Zhang and Sclaroff, 2013]	2013	Probabilistic
DCTS	[Hou et al., 2011]	2011	Fourier/Spectral
CASD	[Goferman et al., 2010]	2010	Biological/Probabilistic
PFT	[Hou and Zhang, 2007]	2007	Fourier/Spectral
PQFT	[Guo et al., 2008]	2008	Fourier/Spectral
QDCT	[Schauerte and Stiefelhagen, 2012]	2012	Fourier/Spectral
SIMgrouping	[Murray et al., 2013]	2013	Biological/Cognitive
RARE	[Riche et al., 2012]	2012	Information-Theoretic
SR	[Hou and Zhang, 2007]	2007	Fourier/Spectral
SUN	[Zhang et al., 2008]	2008	Probabilistic
SeoMilanfar	[Seo and Milanfar, 2009]	2009	Biological/Cognitive
Spratling	[Spratling, 2011]	2011	Biological/Cognitive
Simpsal	[Harel, 2012]	2012	Biological/Cognitive
ML_Net	[Cornia et al., 2016]	2016	Biological/Deep Neural Network
DeepGazeII	[Kümmerer et al., 2016]	2016	Biological/Deep Neural Network

The rest of this paper is organized as follows: Section II introduces the concept of opponent color space, wavelet decomposition, wavelet energy map estimation, and CSF, Section III introduced the model predict saliency map with

different datasets and the details of evaluating metric from mathematics views. Section IV introduces the experiment results. The final section gives conclusions for the paper.

2 The Proposed Saliency Prediction Model

2.1 Saliency Prediction Model

The biological like visual saliency prediction map is proposed inspired by the human low-level visual system. The information extraction in the retina, LGN, and V1 is the fundamental component of the optical neural network. The proposed model architecture mainly contained color opponent channel, wavelet transform, wavelet energy map and contrast sensitivity function. The color opponent channel simulates the retina cells to respond to different spectral wavelengths, and wavelet transforms mainly simulates the V1 multi-scale, multi-orientation properties. The CSF mainly simulates the human brain's susceptibility to spatial frequency. The details of each component will be described in the following contents, respectively. The computational saliency prediction model architecture is illustrated as follows (see Fig.1):

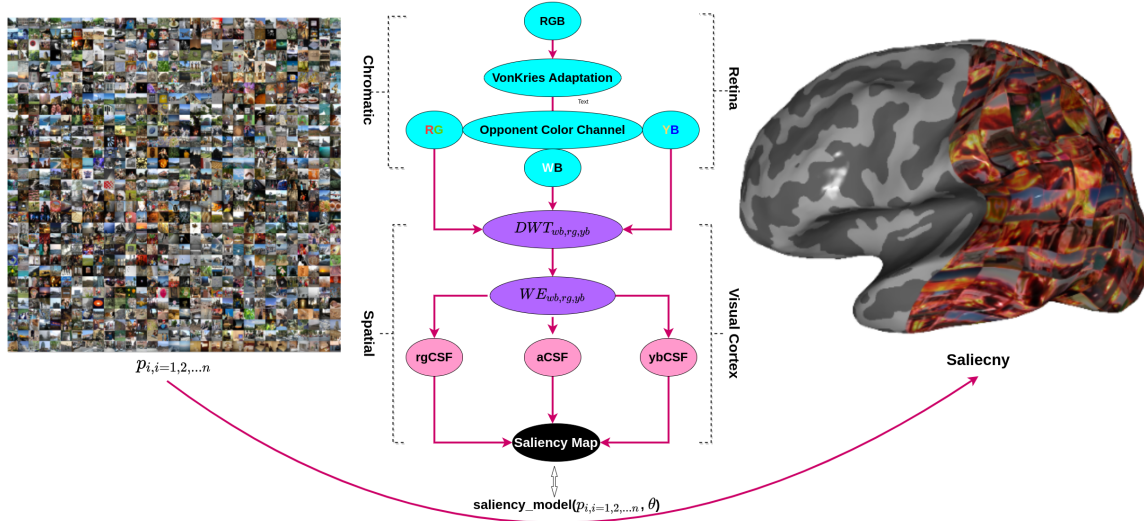


Figure 1: The architecture of proposed saliency prediction model. The left panel image from MIT1003 dataset. The right graph refers to map left panel image saliency prediction on the inflated brain surfer. i and θ indicate image and parameters in the model, respectively.

2.2 Gain control with Von-Kries chromatic adaptation model

Gain control theory widely used in cognitive psychology, its densely related human dynamic behavior [Mercy, 1981]. In the visual information processing pipeline, gain control exists in the retina and cortex. In other words, gain control influences the top-down and bottom-up visual information flow or attention-related cognitive function [Butz, 2004]. Meanwhile, the gain control always drives to maintain a steady-state of brain, and self-regulation condition between the brain and natural environment. In the Von-Kries model, we simply will multiply each channel of the image with a gain after normalizing its individual intensity [Finlayson et al., 1993, 2002, Krauskopf and Gegenfurtner, 1992]. However,

note that there are some implications in this approach. The first one is that the channels are considered independent signals (as Von-Kries proposed), that's why we have independent gains. Second, this gain is added not in the RGB space but in the tristimulus space LMS. Assuming LMS corresponds to the tristimulus values of our image, the von-Kries model mathematically can be expressed as:

$$L_2 = \frac{L_1}{L_{\max}} L_{\max 2}, M_2 = \frac{M_1}{M_{\max}} M_{\max 2}, S_2 = \frac{S_1}{S_{\max}} S_{\max 2} \quad (1)$$

Where L_1 corresponds to original images L values, L_{Max} corresponds to the maximum value or reference white in the original image in the L channel, L_{Max2} is the gain value (or new light condition), and L_2 is the corrected L channel. Same for the other two channels. It can put together then formally represented as:

$$\begin{bmatrix} L_{post} \\ M_{post} \\ S_{post} \end{bmatrix} = \begin{bmatrix} \frac{1}{L_{\max}} & 0 & 0 \\ 0 & \frac{1}{M_{\max}} & 0 \\ 0 & 0 & \frac{1}{S_{\max}} \end{bmatrix} \begin{bmatrix} L_1 \\ M_1 \\ S_1 \end{bmatrix} \quad (2)$$

$$\begin{bmatrix} L_2 \\ M_2 \\ S_2 \end{bmatrix} = \begin{bmatrix} L_{\max 2} & 0 & 0 \\ 0 & M_{\max 2} & 0 \\ 0 & 0 & S_{\max 2} \end{bmatrix} \quad (3)$$

2.3 Color Appearance Model

In this section, we will describe the color opponent channel in the proposed model. Color representation in the brain can significantly improve object recognition and identity and reduce redundancy. As we said before, visual information input from the natural environment includes heavy redundancy [Barlow, 1990]. The Trichromatic Theory [Brill, 2014] and the color appearance model proposed, which is inspired by low-level human visual system function, helps us understand how the sensors encode color information and widely used in low-level image processing. The two functional types of chromatic sensitivity or selectivity sensors were found: Single-Opponent and Double-Opponent neurons based on long (L), mediate (M), short (S) cones response in the physical light world [Shapley and Hawken, 2011].

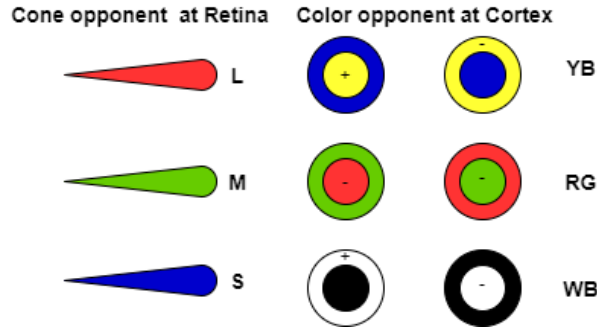


Figure 2: The receptive field of opponent color space "+" indicate excitation, "-" represent inhibition.

The most of saliency predicts model used opponent color space is CIE Lab and YUV color space. In our case, we were introducing a new opponent color space proposed by Hering in 1957 [Hurvich and Jameson, 1957]. The color space from RGB to $O_1O_2O_3$ transform matrix can be expressed as:

$$\begin{bmatrix} O_1 \\ O_2 \\ O_3 \end{bmatrix} = \begin{bmatrix} 0.2814 & 0.6938 & 0.0638 \\ -0.0971 & 0.1458 & -0.0250 \\ -0.0930 & -0.2529 & 0.4665 \end{bmatrix} \begin{bmatrix} sR \\ sG \\ sB \end{bmatrix} \quad (4)$$

The test nature scene images (size are 256x256, 512x512) were selected from Signal and Image Processing Institute, University of Southern California ⁶ and Kodak lossless true color image database ⁷(size are 512x768, 768x512, 768x512). The total nature color images are resized into the same size (8 bits, 256x256) as test images (see Fig.3).

⁶<http://sipi.usc.edu/database/database.php?volume=misc>

⁷<http://r0k.us/graphics/kodak/>

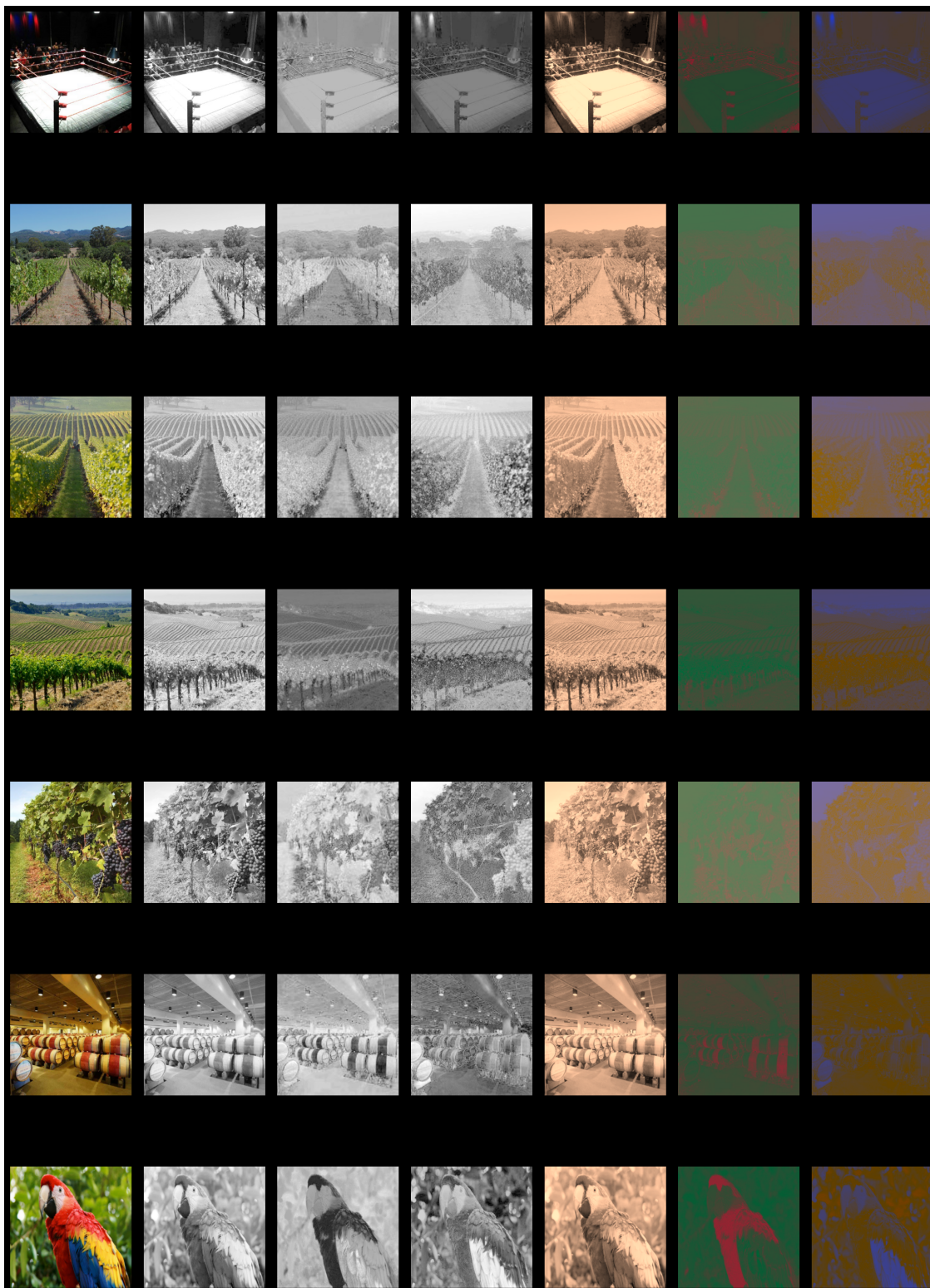


Figure 3: Color opponent processing. The first column denotes raw RGB color space, then follow the White-Black (WB) channel, Red-Green (RG) channel, and Yellow-Blue (YB) channel with a gray colormap, respectively. The last three columns also represent the WB, RG, and YB channels with artificial color for better to visualize opponent processing at the visual cortex level.

2.4 Wavelet Energy Map

The wavelet image analysis can be decomposed image into multi-scale and multi-orientation features similar to visual cortex representation. Compared to the Fourier Transform (FT), WT can represent spatial and frequency information simultaneously. Alfred Haar first proposed the WT approach, and it has already been widely used in signal analysis [Haar, 1912], e.g., image compression, image de-noising, classification. WT also was already applied in the visual saliency map prediction and achieved good performance [imamoğlu et al., 2013]. However, WE are still barely used in the visual saliency map prediction, and it can be used to enhance local contrast information in the decomposition sub-bands. Discrete Wavelet Transform (DWT) used in our proposed model and its basic principle can be mathematically expressed as:

$$r[n] = ((I * f)[n]) \downarrow 2 = \left(\sum_{k=-\infty}^{\infty} I[k]f[n-k] \right) \downarrow 2 \quad (5)$$

Where I indicates input images, f represents a series of filter banks (low-pass and high-pass), and $\downarrow 2$ indicates down-sampling until the next layer signal cannot be decomposed any more (see Fig.4). A series of sub-band images are produced after convolution with DWT, and then WE can be calculated from each sub-band features (see Fig.5).

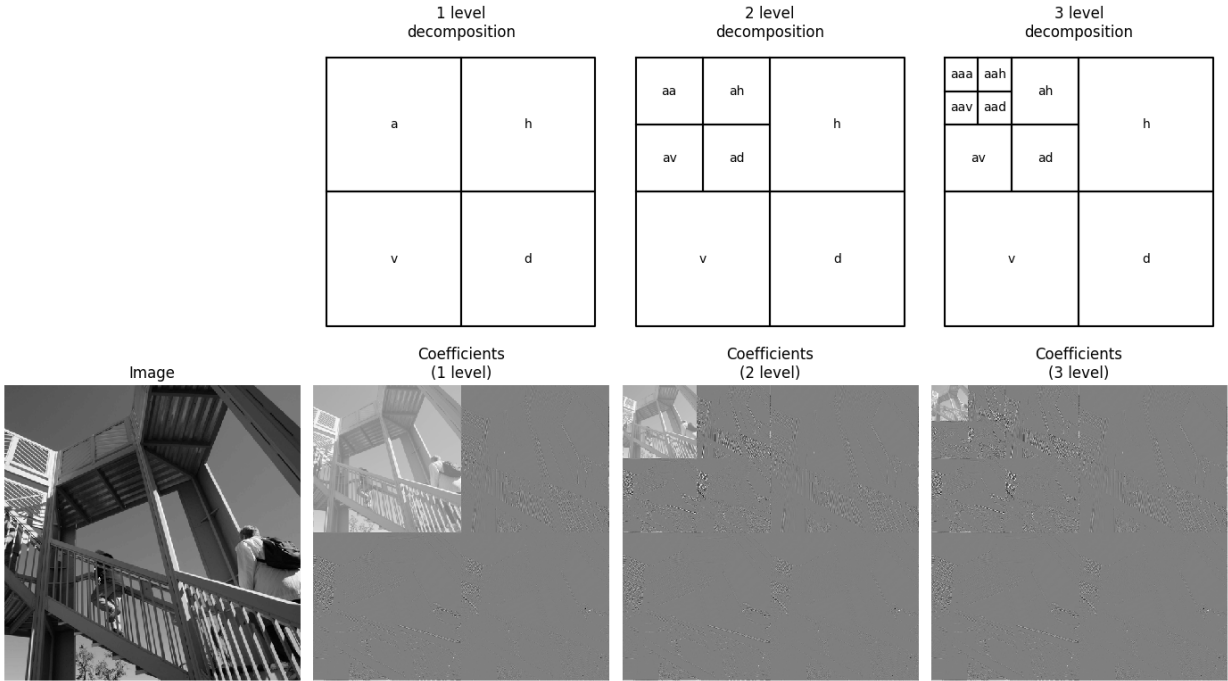


Figure 4: The different decomposition levels with DWT. e.g. 1 level, 2 level and 3 levels. 'a' indicates original image, 'h' indicates horizontal features, 'v' for vertical features and 'd' represent diagonal feature, respectively.

The wavelet energy map can be expressed as:

$$\mathcal{WE}(i, j) = \|I(i, j)\|^2 = \sum_{k=1}^{3ind+1} |I_k(i, j)|^2 \quad (6)$$

Where ind indicates the maximum level of an image can be decomposed in the last, and $I_k(i, j)^2$ represents the energy map of each sub-band features.

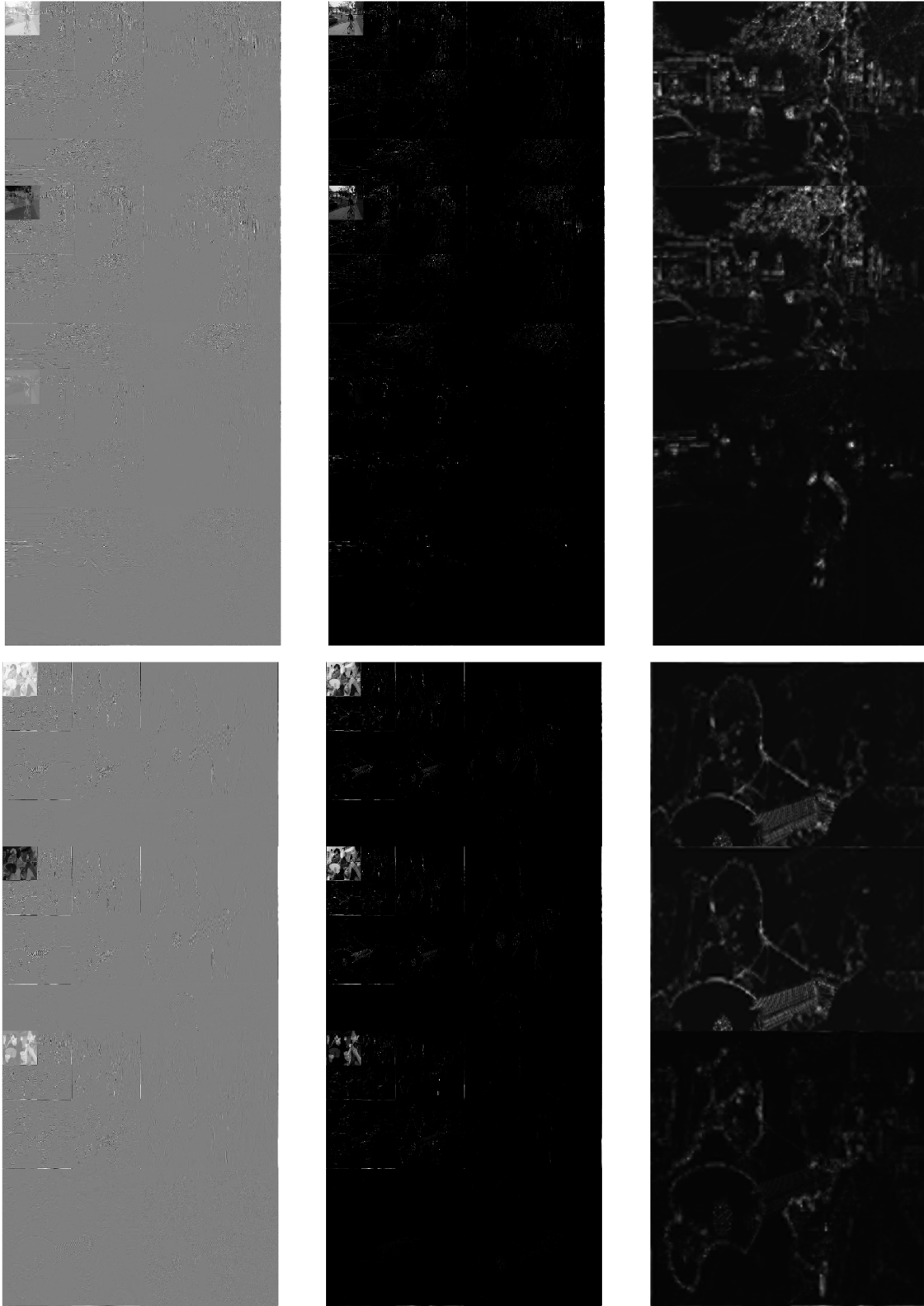


Figure 5: Each channel DWT maps and its corresponded WE maps. The first column refers to DWT maps for achromatic (WB) and chromatic(RG, YB) channels and second column indicates WE maps for WB, RG and YB opponent channel, respectively.

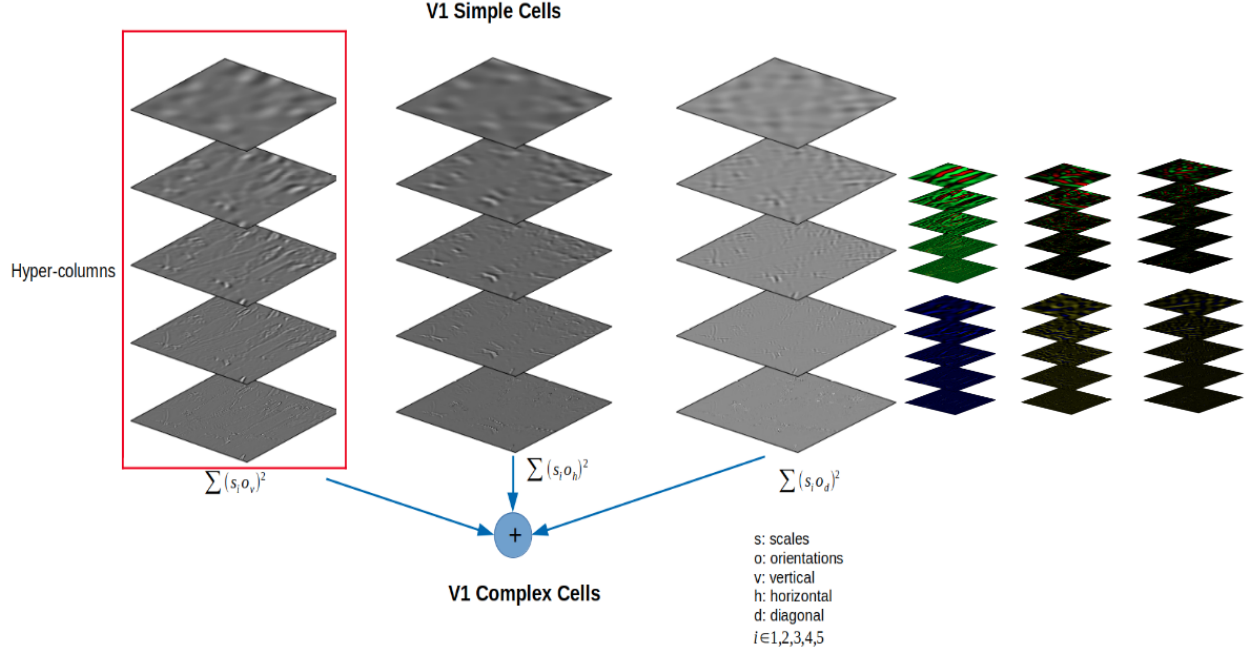


Figure 6: The model of V1 simple and complex cells

2.4.1 The visual cortex receptive fields with wavelet filters

The visual simple and complex cells can be modeling with wavelet filters. In our case, we not considered in-depth details of each hyper-column neuron interactions mechanisms (e.g., Li's model [Zhaoping, 1998]). The V1 complex receptive fields simulated sum all squares of different scales and orientations after wavelet transform (see Fig.6).

The V1 simple receptive fields mathematically defined as:

$$V_{1i,i=1,2\dots5} = S_{i,i=1,2\dots5} O_v \quad V_{1i} = S_i O_h \quad V_{1i} = S_i O_d \quad (7)$$

Where S indicates receptive filed scales, o refers to orientation (e.g. vertical (v), horizontal (h), and diagonal (d), respectively.) Followed V1 complex cells can be formula as:

$$V_2 = \sum_i^5 (S_i O_v)^2 + \sum_i^5 (S_i O_h)^2 + \sum_i^5 (S_i O_d)^2 \quad (8)$$

2.5 Contrast Sensivity Function

The human visual system is compassionate of contrast change in the natural environment. The visual cortex function can be decompose into subset compositions, and one of the significant features is CSF. It can be divided into achromatic and chromatic spatial CSFs [Mullen, 1985]. In this proposed computational modeling, achromatic CSF (aCSF) and chromatic CSFs (rgCSF and ybCSF) was implemented into the model, which was firstly proposed by Mannos and Sakrison in 1974 [Mannos and Sakrison, 1974] then improved later [Watson and Malo, 2002, Watson and Ahumada, 2010] (see Fig.7). The achromatic CSF mathematics can be expressed as:

$$\text{CSF}(fx, fy) = T(f) * O(fx, fy) \quad (9)$$

$$T(f) = g * (\exp(-(f/f_m)) - l * \exp(-(f^2/s^2))) \quad (10)$$

$$O(fx, fy) = 1 - w * (4(1 - \exp(-(f/os))) * fx^2 * fy^2) / f^4 \quad (11)$$

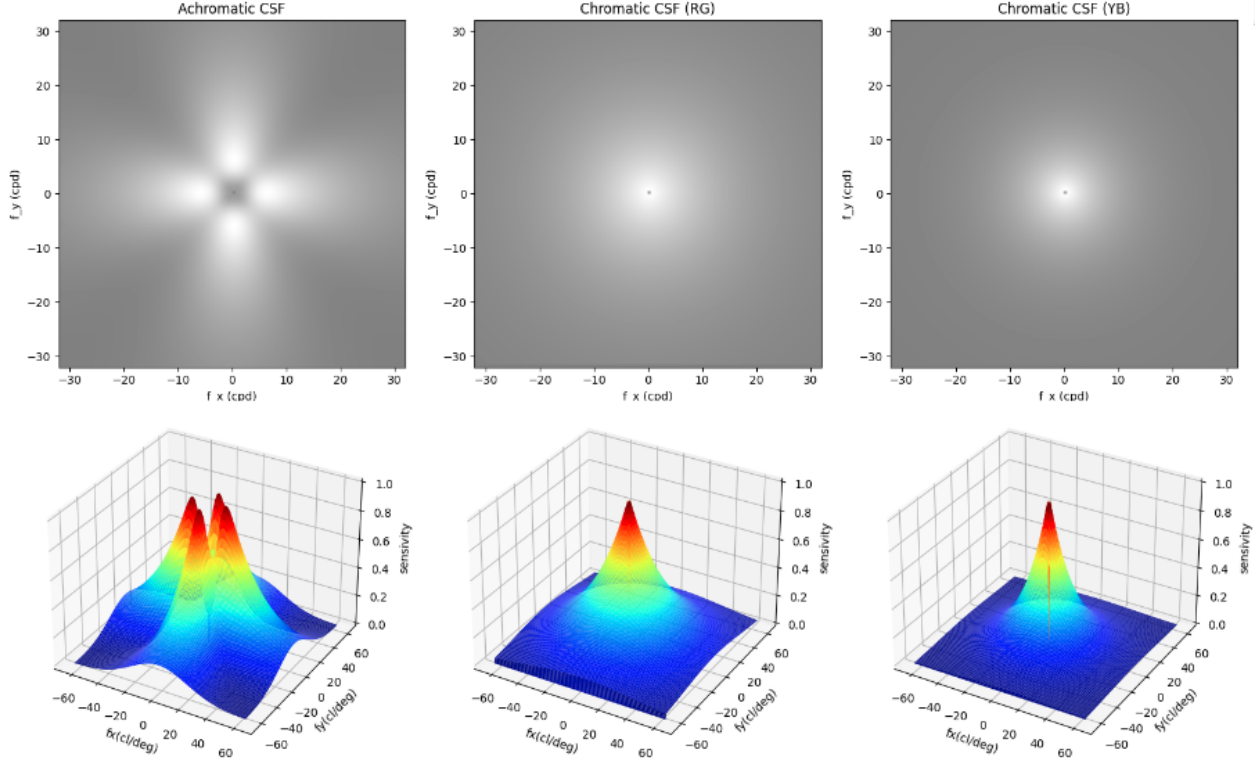


Figure 7: Achromatic and Chromatic CSF. The top image refers to 2D CSFs and bottom row indicates 3D CSFs.

Where (f_x, f_y) indicates 2D spatial frequency vector (in cycle/deg), f represents modulus of the spatial frequency (in cycle/deg), g represents overall gain ($g = 330.74$), f_m indicates parameter that control the exponent decay of the CSF Tyler ($f_m = 7.28$), l represents loss at low frequencies ($l = 0.837$), s indicates parameter that control the attenuation of the loss factor at high frequencies ($s = 1.809$), w indicates weighting of the Oblique Effect ($w = 1$), os indicates Oblique Effect scale ($os = 6.664$).

The CSF is applied with the WE image in the Fourier domains. It can be the formula as:

$$CSF_{WE} = real(\mathcal{F}(\mathcal{I}(\mathcal{F}(WE.real)) \otimes CSF))) \tag{12}$$

Where \mathcal{F} indicates 2D Fourier transform, \mathcal{F} indicates 2D inverse Fourier transform, \mathcal{I} indicates *fftshift* and \mathcal{I} indicates *ifftshift*. My Python implementation of above CSF (aCSF, rgCSF and ybCSF) are available at <https://github.com/sinodanish/CSFpy>.

3 Materials and Methods

3.1 Datasets

The proposed model was evaluated on several well-known datasets, including MIT1003, MIT300, TORONTO, and SID4VAM, described below.

3.1.1 MIT1003

MIT1003 is an image dataset that includes 1003 images from the Flickr and LabelMe collections (see Fig.8). The fixation map was generated from recording 15 participants’ eye-tracking data. It is the largest eye tracking dataset. The dataset includes 779 landscapes and 228 portraits of images which size spanning from 405×405 to 1024×1024 pixels [Judd et al., 2012].

3.1.2 MIT300

MIT300 is a benchmark saliency test dataset that includes 300 images from recoding 39 observers' eye-tracking dataset (see Fig.8). The MIT300 dataset categories are highly varied and natural. The dataset can be used for model evaluation [Judd et al., 2012].

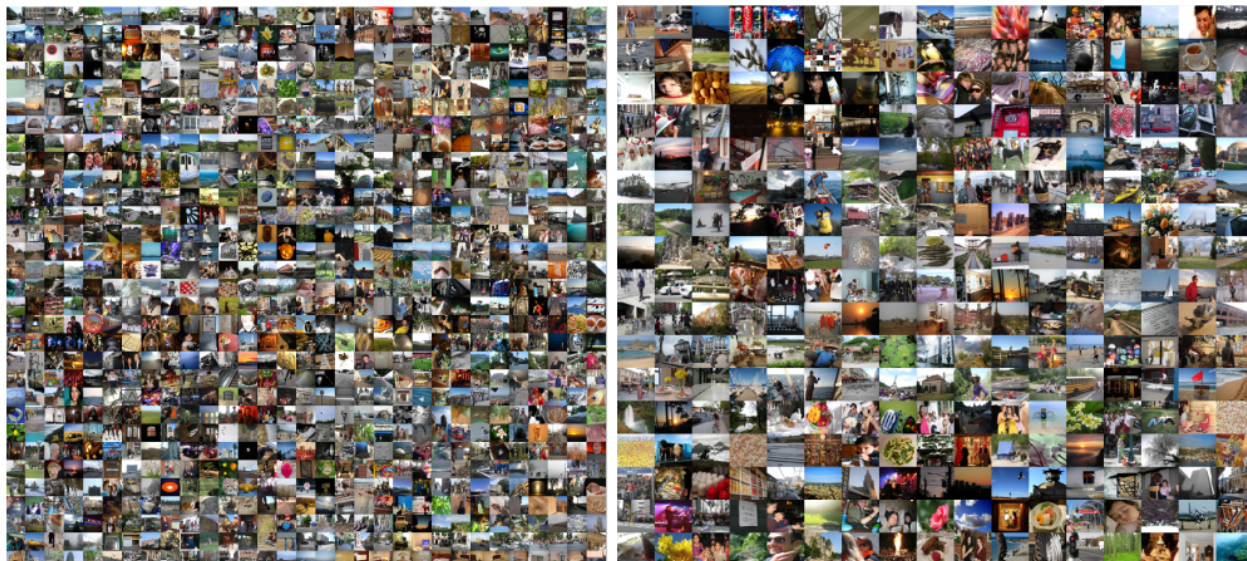


Figure 8: MIT1003 and MIT300 datasets

3.1.3 TORONTO

The TORONTO dataset included 120 chromatic images and was free-viewed by 20 subjects (see Fig.9). The datasets contained both outdoor and indoor scenes with a fixed resolution of 511×681 pixels [Bruce and Tsotsos, 2005].

3.1.4 SID4VAM

SID4VAM is a synthetic image database that is mainly used to psycho-physical evaluate the V1 properties (see Fig.9). The database is composed of 230 synthetic images. It includes 15 distinct types of low-level features (e.g., brightness, size, color, and orientation, etc.) with different a target-distractor pop-out type of synthetic images [Berga et al., 2019].

3.2 Evaluation Metrics

There are several approaches, as we mentioned before, to evaluate metrics between visual saliency and model prediction. In general, saliency evaluation can be divided into two branches that location-based and distribution-based respective. The former mainly focuses on the district located in the saliency map, and the latter considers both predicted saliency and human eye fixation maps as continuous distributions [Bylinskii et al., 2016]. In this research, we used AUC, NSS, CC, SIM, IG, and KL to evaluate methods and details of each evaluate metric described as follow sections ⁸.

3.2.1 Area under ROC Curve (AUC)

The AUC metric is one of the popular approaches to evaluate saliency model performances. The saliency map can be treated as a binary classifier to split positive samples from negative samples by setting different thresholds. The actual positive (TP) is the saliency map values' proportion beyond a specific threshold at the fixation locations. In verse, false positive (FP) is the saliency map values' proportion beyond a specific threshold at the non fixation locations. In our case, the thresholds are set from the saliency map values and AUC-Judd, AUC-Borji and sAUC measured [Borji et al., 2013].

⁸<https://github.com/cvzoya/saliency>

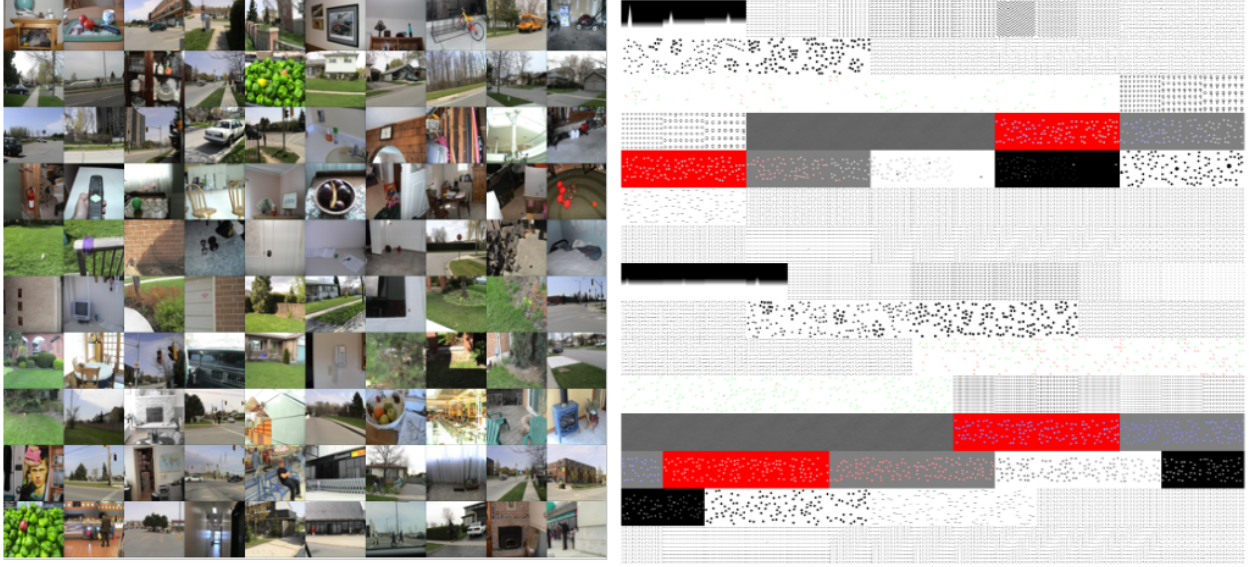


Figure 9: TORONTO and SID4VAM datasets

3.2.2 Normalized Scanpath Saliency (NSS)

The NSS metric usually measured the relationship between human eye fixation maps and model prediction saliency maps [Emami and Hoberock, 2013]. Given a binary fixation map F and saliency map S , The NSS can be formally defined as:

$$NSS = \frac{1}{N} \sum_{i=1}^N \bar{S}(i) x F(i) \quad (13)$$

$$N = \sum_i F(i) \text{ and } \bar{S} = \frac{S - \mu(s)}{\sigma(S)} \quad (14)$$

Where N is the total number of human eye positions and $\sigma(S)$ is the standard deviation.

3.2.3 Similarity Metric (SIM)

The similarity metric (SIM) is a very famous algorithm from measure image structure similarity, and it has already widely used in image quality and image processing disciplines [Riche et al., 2013]. The SIM mainly measured the normalized probability distributions of eye fixation and model prediction saliency maps. The SIM can be mathematically described as:

$$SIM = \sum_{i=1} \min(P(i), Q(i)) \quad (15)$$

Where $P(i)$ and $Q(i)$ are the normalized saliency map and the fixation map, respectively. A similarity score should be located between zero and one.

3.2.4 Information Gain (IG)

The information gain is an approach to measure saliency map prediction accuracy from the information-theoretic view. It mainly measured the critical information contained in the predict saliency map compared with the ground truth map [Kümmerer et al., 2015a]. The mathematical formula of IG can be expressed as:

$$IG(P, Q^B) = \frac{1}{N} \sum_i Q_i^B [\log_2(\epsilon + P_i) - \log_2(\epsilon + B_i)] \quad (16)$$

Where P indicate prediction saliency map, and Q^B is baseline map, ϵ represents regularity parameters.

3.2.5 Pearson’s Correlation Coefficient (CC)

Pearson’s Correlation Coefficient (CC) is one of the linear approaches that measured how many similarities between prediction saliency map and baseline map [Jost et al., 2005].

$$CC(P, Q^D) = \frac{\sigma(P, Q^D)}{\sigma(P) \times \sigma(Q^D)} \quad (17)$$

Where P indicates prediction saliency map and Q^D is the ground truth saliency map.

3.2.6 Kullback-Leibler divergence (KL)

The Kullback-Leibler divergence (KL) was used to measure two distribution samples’ distance from information-theoretic views [Kümmerer et al., 2015a]. It can be formally defined as:

$$KL(P, Q^D) = \sum_i Q_i^D \log \left(\epsilon + \frac{Q_i^D}{\epsilon + P_i} \right) \quad (18)$$

Where P indicates prediction saliency map and Q^D is the ground truth saliency map. ϵ also represents regularity parameters.

3.2.7 Other metrics

We also evaluate different salient prediction models’ performance through two main metrics, including the precision-recall curves (PR curves), F-measure⁹. By binarizing the predicted saliency map with thresholds in [0,255], a series of precision and recall score pairs is calculated for each dataset image. The PR curve is plotted using the average precision and recall of the dataset at different thresholds either [Feng, 2018].

4 Experimental Results

4.1 Quantitative Comparison of the Proposed Model with other State-of-the-Art Models

To evaluate the performance of the proposed model, we compared it with the other eight state-of-the-art models. We selected MIT1003 and SID4VAM benchmarks for a comparison of the quantitative results. These results were reported in Table 1, Table 2, Table 3 and Fig.15.

⁹https://github.com/ArcherFMY/sal_eval_toolbox/

Methods	DNN	AUC_Judd	AUC_Borji	sAUC	NSS	SIM
ITT	B	0.674	0.655	0.610	0.629	0.291
WECSF	N	0.705	0.692	0.653	0.849	0.362
SR	N	0.708	0.683	0.638	0.791	0.329
AIM	N	0.706	0.696	0.639	0.780	0.282
BMS	N	0.684	0.637	0.576	0.729	0.346
CASD	N	0.747	0.731	0.651	0.977	0.350
DCTS	N	0.746	0.732	0.650	1.000	0.322
HFT	N	0.797	0.764	0.619	1.258	0.416
ICL	N	0.769	0.713	0.617	1.048	0.420
PFT	N	0.708	0.683	0.636	0.787	0.326
PQFT	N	0.643	0.530	0.519	0.459	0.292
QDCT	N	0.736	0.714	0.647	0.920	0.338
RARE	N	0.777	0.755	0.665	1.198	0.380
SIM	N	0.701	0.693	0.653	0.743	0.283
SUN	N	0.665	0.647	0.601	0.629	0.287
Achanta	N	0.534	0.526	0.526	0.174	0.240
Simpsal	N	0.735	0.721	0.610	0.892	0.337
Spratling	N	0.512	0.508	0.510	0.039	0.234
SIMgrouping	N	0.724	0.716	0.668	0.873	0.308
SeoMilanfar	N	0.710	0.688	0.633	0.808	0.351
ML_Net	Y	0.836	0.743	0.689	1.928	0.565
DeepGazeII	Y	0.886	0.837	0.779	2.483	0.527

Table 1: Quantitative scores of several models for the MIT1003 dataset. The baseline ITT model are SkyBlue-hatched and proposed model are Green-hatched. The black bold scores indicate best performance of saliency prediction models. 'N' indicates NO and vice versa, 'B' indicate Baseline. The results of MIT1003 dataset of ML_Net and DeepGazeII are pink-hatched because the dataset is used to train ML_Net and DeepGazeII and cannot be compared with other models.

Methods	DNN	AUC_Judd	AUC_Borji	sAUC	NSS	SIM
ITT	B	0.700	0.679	0.641	0.816	0.317
WECSF	N	0.701	0.686	0.674	0.844	0.365
SR	N	0.744	0.722	0.683	1.019	0.343
AIM	N	0.727	0.718	0.664	0.885	0.356
SIM	N	0.754	0.744	0.707	0.951	0.361
SUN	N	0.674	0.653	0.613	0.656	0.285
HFT	N	0.820	0.792	0.659	1.548	0.522
ICL	N	0.792	0.737	0.652	1.245	0.532
PFT	N	0.742	0.717	0.684	1.001	0.339
CASD	N	0.780	0.764	0.688	1.237	0.364
PQFT	N	0.650	0.524	0.517	0.482	0.263
QDCT	N	0.769	0.748	0.691	1.174	0.354
RARE	N	0.806	0.774	0.693	1.514	0.402
Achanta	N	0.551	0.541	0.539	0.249	0.305
Simpsal	N	0.769	0.754	0.648	1.121	0.355
Spratling	N	0.508	0.503	0.509	0.015	0.242
SIMgrouping	N	0.769	0.760	0.710	1.090	0.326
SeoMilanfar	N	0.769	0.744	0.695	1.185	0.382
ML_Net	Y	0.823	0.803	0.750	1.824	0.536
DeepGazeII	Y	0.846	0.827	0.756	2.199	0.620

Table 2: Quantitative scores of several models for the Toronto dataset. The baseline ITT model are SkyBlue-hatched and proposed model are Green-hatched. The black bold scores indicate best performance of saliency prediction models. The results of Toronto dataset of ML_Net and DeepGazeII are pink-hatched because the dataset is used to train ML_Net and DeepGazeII and cannot be compared with other models either.

Models	DNN	AUC_Judd	AUC_Borji	sAUC	CC	NSS	KL	SIM	IG
GT	B	0.943	0.882	0.860	1.000	4.204	0.000	1.000	2.802
Baseline-CG	B	0.703	0.697	0.525	0.281	1.577	0.722	0.372	-0.189
ITT	B	0.645	0.592	0.591	0.165	0.801	1.778	0.315	-0.104
WECSF	N	0.667	0.647	0.646	0.378	1.019	1.769	0.459	-1.508
AIM	N	0.572	0.566	0.560	0.118	0.515	14.96	0.216	-18.742
Achanta	N	0.505	0.513	0.513	0.060	0.334	8.431	0.117	-9.634
BMS	N	0.811	0.517	0.515	0.129	0.702	19.161	0.624	-24.258
CASD	N	0.737	0.673	0.663	0.429	2.124	2.659	0.397	-1.263
DCTS	N	0.732	0.725	0.715	0.440	2.191	1.442	0.377	0.363
HFT	N	0.780	0.753	0.697	0.561	2.364	1.424	0.458	0.406
ICL	N	0.742	0.716	0.630	0.344	1.189	1.974	0.391	-0.443
PFT	N	0.704	0.692	0.688	0.407	2.074	2.556	0.361	-1.230
PQFT	N	0.581	0.518	0.517	0.112	0.611	12.262	0.175	-15.074
QDCT	N	0.717	0.705	0.699	0.419	2.139	1.850	0.368	-0.213
SIM	N	0.648	0.638	0.628	0.181	0.744	1.799	0.340	-0.152
SR	N	0.747	0.695	0.689	0.423	2.087	1.508	0.414	0.354
SUN	N	0.545	0.536	0.535	0.086	0.403	17.387	0.155	-22.268
Simpsal	N	0.753	0.740	0.661	0.370	1.380	1.461	0.393	0.323
Spratling	N	0.535	0.527	0.534	0.030	0.176	17.801	0.147	-22.890
SIMgrouping	N	0.649	0.638	0.638	0.191	0.866	1.925	0.350	-0.338
SeoMilanfar	N	0.703	0.692	0.698	0.246	1.181	2.696	0.337	-1.400
ML_Net	Y	0.600	0.593	0.501	0.118	0.341	7.529	0.370	-2.153
DeepGazeII	Y	0.645	0.581	0.475	0.103	0.555	2.450	0.274	-1.128

Table 3: Quantitative scores of several models for the SID4VAM dataset. The baseline ITT model are LightBlue-hatched and proposed model are Green-hatched. The black bold scores indicate best performance of saliency prediction models. The Fourier/Spectral inspired models has the best prediction scores compared to other start-of-the-art non-neural network and even deep neural network models on the SID4VAM dataset. The results of SID4VAM dataset of ML_Net and DeepGazeII are pink-hatched because the dataset is used to train ML_Net and DeepGazeII and cannot be compared with other models either.

4.2 Qualitative Comparison of the Proposed Model with Other State-of-the-Art Models

We qualitatively tested the proposed model with the MIT1003, MIT300, TORONTO, SID4VAM and UCF Sports dataset, respectively. Meanwhile, we compared the model performance with other state-of-the-art saliency prediction modelings on the MIT1003, TORONTO and SID4VAM datasets. Fig.10, 11, 12, 13 and 14 illustrate the saliency map results obtained when the proposed model and other state-of-the-art models are applied to sample images drawn from the studied dataset. We can see that the proposed model can predict most of the salient objects in the given images. Furthermore, the proposed model can successfully detect the orientation, boundary, and pop out function when the model applied the SID4VAM dataset.



Figure 10: Performance evaluation with MIT1003 database. The first row is color images, second row is ground truth saliency map and the last row is proposed model prediction saliency map.

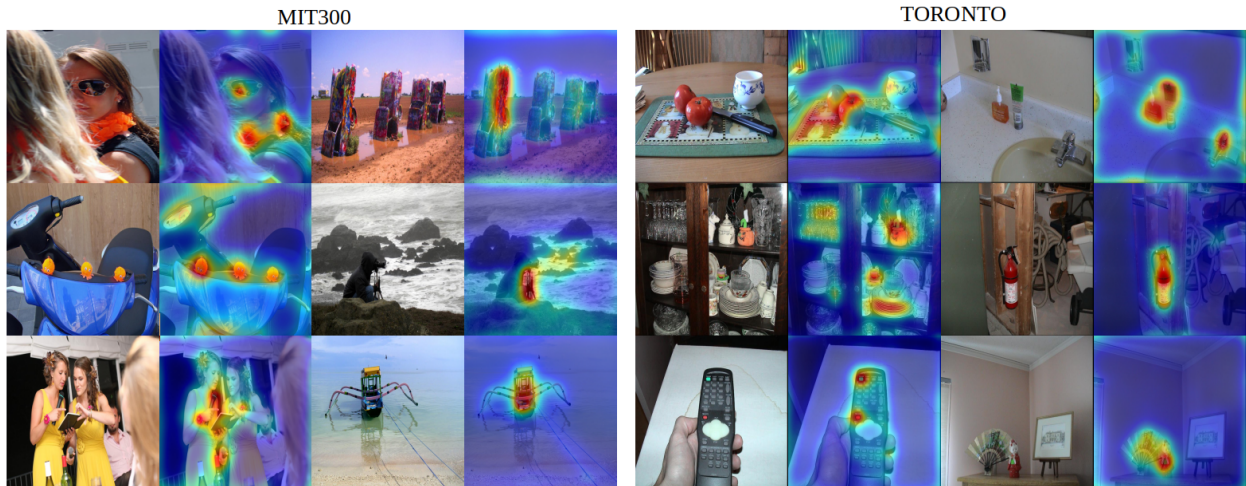


Figure 11: Left:Performance evaluation with MIT300 database. The first and third column is color images. The second and fourth column is proposed model prediction saliency maps. Right:Performance evaluation with TORONTO database. The first and third column is color images. The second and fourth column is proposed model prediction saliency maps either.

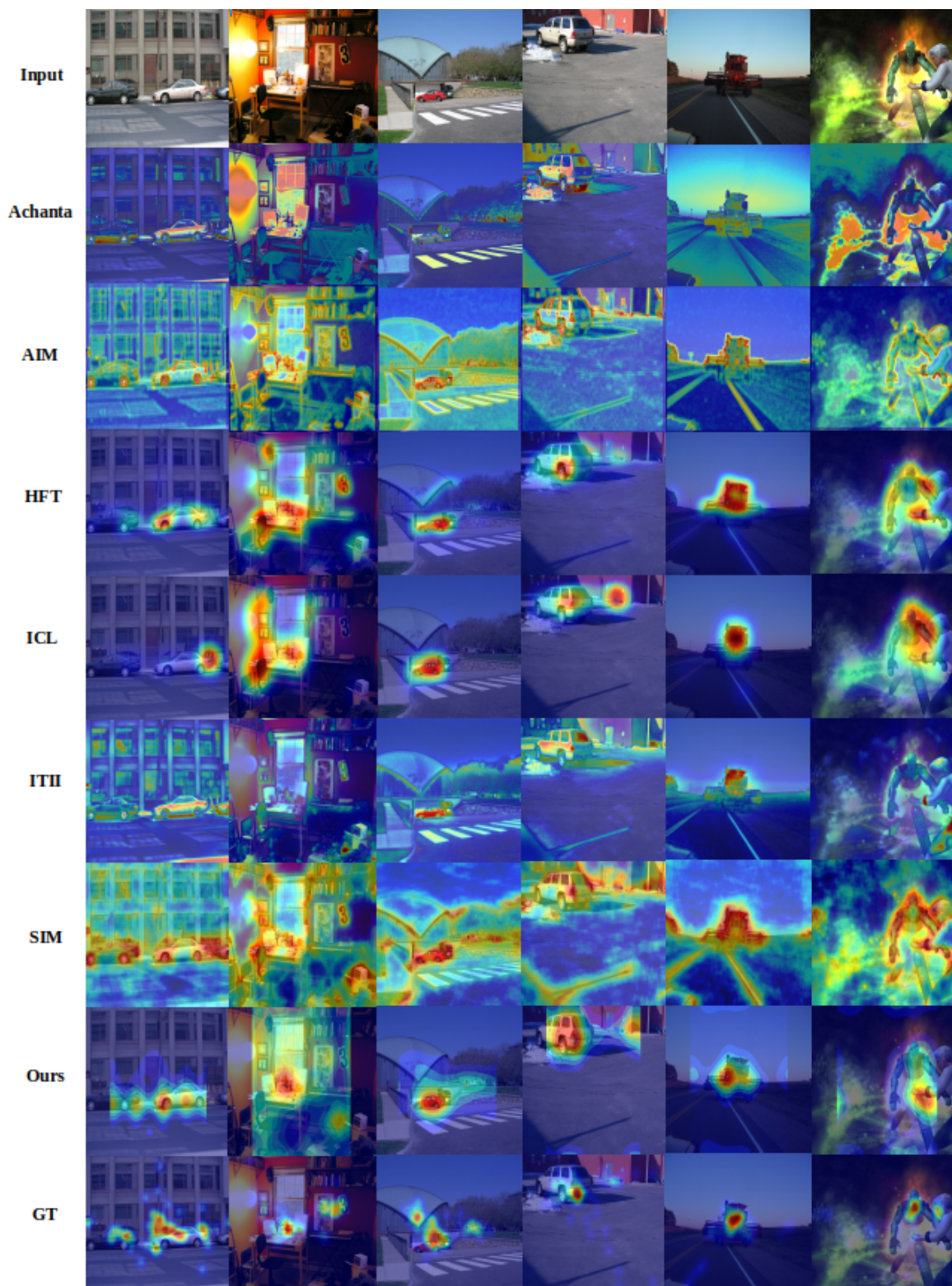


Figure 12: Qualitative saliency prediction results from MIT1003 database with selected different models. The first row is six stimuli images selected from the MIT1003 database. Then follow with Achanta, AIM, HFT, ICL, ITII, SIM, Proposed models, and Ground Truth (GT) saliency prediction result with artificial color for better visualization.

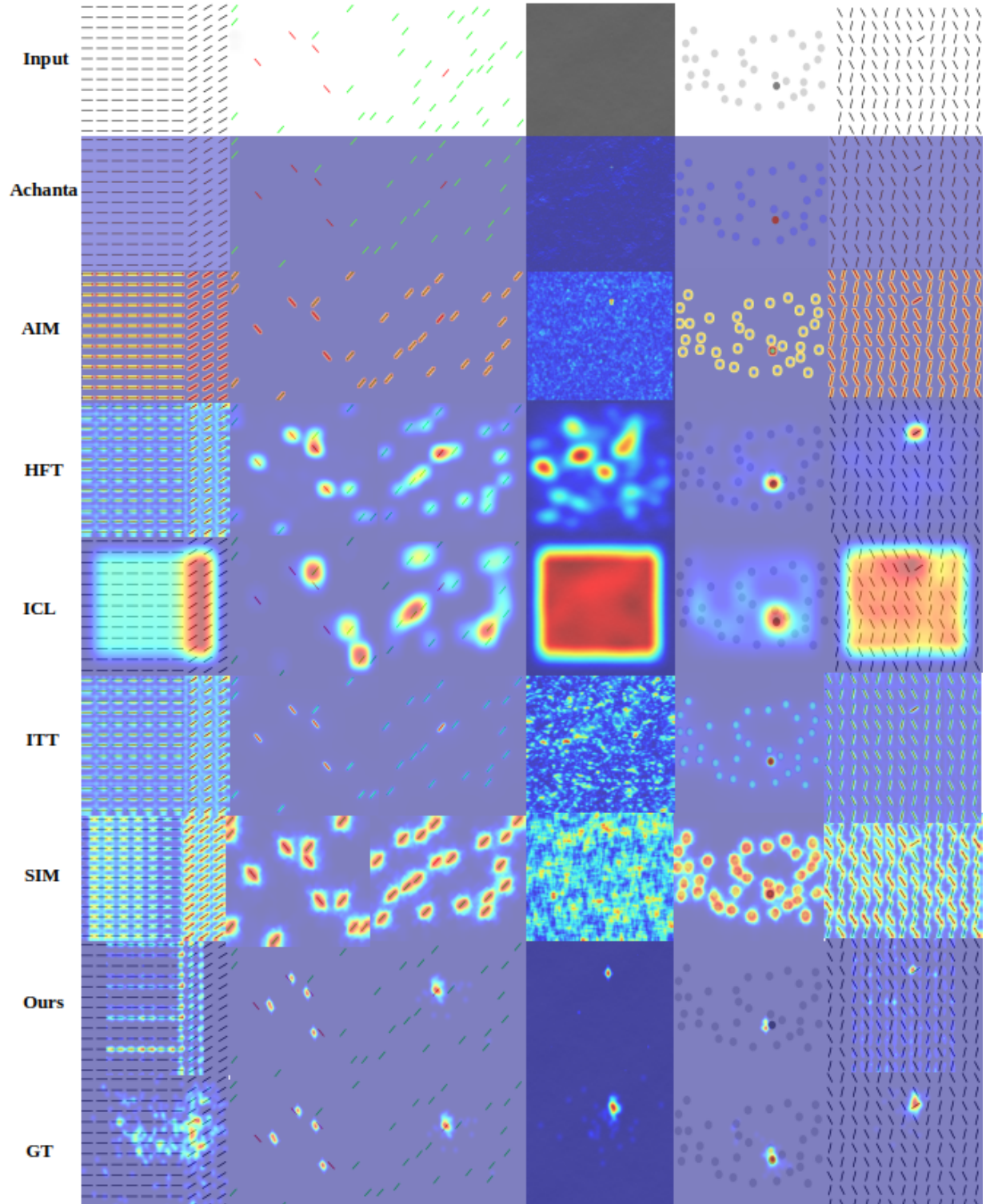


Figure 13: Qualitative saliency prediction results from SID4VAM database with selected different models. The first row is six stimuli images selected from the SID4VAM database. Then follow with Achanta, AIM, HFT, ICL, ITT, SIM, Proposed models, and Ground Truth (GT) saliency prediction result with artificial color for better visualization. The proposal model can be successfully applied to explain "pop out" effect in visual search.

Frames=1:28

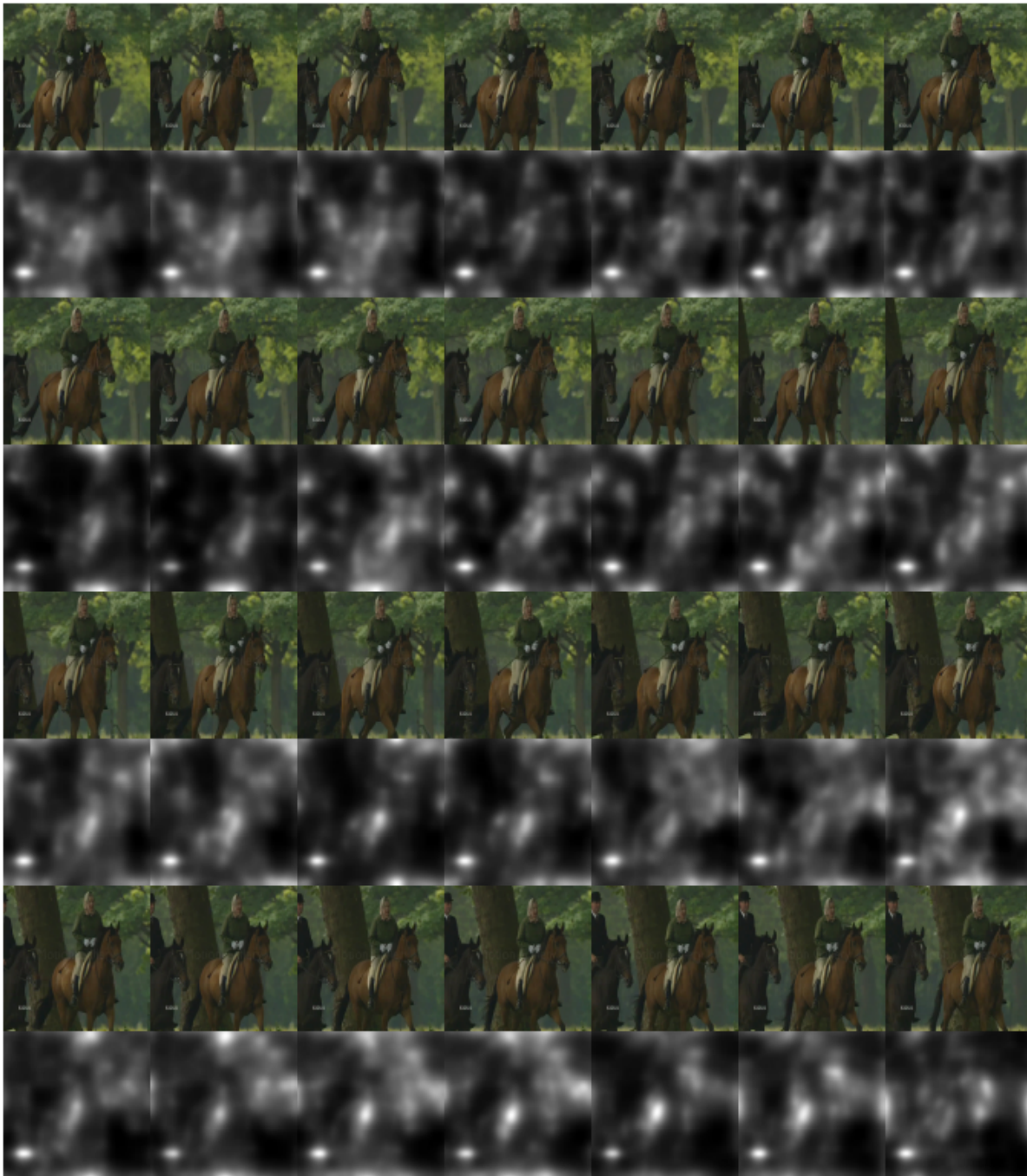


Figure 14: Dynamic saliency prediction. For these sample frames from UCF Sports Action Dataset. The model clearly produces better results and perfectly captures the left-bottom text information.

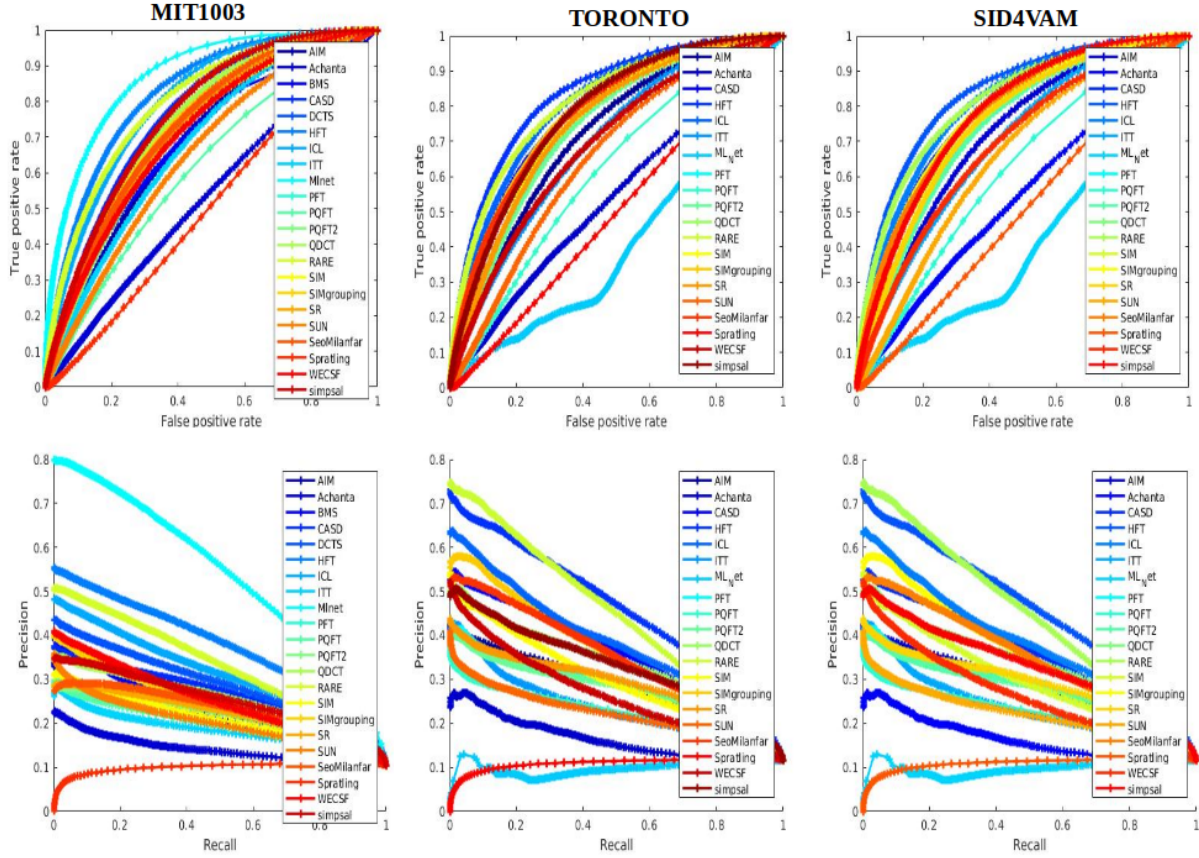


Figure 15: Comparison of the area-under-the-curve (AUC) and PR curves with different thresholds of our method and other state-of-art methods on three benchmark datasets.

5 Conclusions

In this study, an HVS-Oriented computational visual saliency prediction modeling has been proposed, inspired by a low-level human visual pathway. This study uses color opponent channel, wavelet transform, wavelet energy map, and contrast sensitivity functions to predict saliency map. The model was evaluated by classical benchmark datasets and achieved good outperforms of visual saliency prediction compared with baseline model. Furthermore, our model inspired by human vision system then go-back use model performance to help us understand the brain function, it is loop program and we also confirmed Fourier/Spectral inspired saliency prediction models has the best prediction scores compared to other start-of-the-art non-neural network and even deep neural network models on the simple image features saliency prediction. Deep neural network has out-performance on the nature image salient prediction but worse performance on the simple images, but Fourier/Spectral inspired model has opposite effect because Fourier/Spectral inspired model simulated the optical neural processing from retina to V1 and deep neural network starting from V1 to temporal vision cortex function. Finally, we also extend our model to spatial-temporal saliency prediction and it can capture most significant feature in the video either.

6 Code availability

The code performs all the experiments described in this article are available when paper officially accepted by Journal.

7 Acknowledgments

This work was funded by the Generalitat Valenciana through the grant GrisoliaP/2019/035.

8 Conflicts of Interest

The authors declare no conflicts of interest.

9 Abbreviations

HSV	Human Vision System
V1	Primary Visual Cortex
CNN	Convolution Neural Network
DNN	Deep Neural Network
WT	Wavelet Transform
IWT	Inverse Wavelet Transform
AUC	Area under ROC curve
NSS	Normalized Scanpath Saliency
CC	Pearson’s Correlation Coefficient
SIM	Similarity or histogram intersection
IG	InformationGain
KL	Kullback–Leibler divergence
CSF	Contrast Sensitivity Function
FT	Fourier Transform
DWT	Discrete Wavelet Transform
IDWT	Inverse Discrete Wavelet Transform
LGN	Lateral Geniculate Nucleus
GT	Ground Truth

References

- R. Achanta, S. Hemami, F. Estrada, and S. Süsstrunk. Frequency-tuned salient region detection. *Proceedings of the IEEE Conference on Computer Vision Pattern Recognition (CVPR)*, 06 2009. doi: 10.1109/CVPR.2009.5206596.
- H. Barlow. Sensory mechanisms, the reduction of redundancy, and intelligence. *Proc. of the Nat. Phys. Lab. Symposium on the Mechanization of Thought Process*, (10):535–539, 1959.
- H. Barlow. *Vision: Coding and Efficiency*, chapter A theory about the functional role and synaptic mechanism of visual aftereffects. Cambridge Univ. Press, Cambridge, UK, 1990.
- D. Berga, X. R. Fdez-Vidal, X. Otazu, and X. M. Pardo. Sid4vam: A benchmark dataset with synthetic images for visual attention modeling. *2019 IEEE/CVF International Conference on Computer Vision (ICCV)*, pages 8788–8797, 2019.
- A. Borji. Saliency prediction in the deep learning era: Successes and limitations. *IEEE transactions on pattern analysis and machine intelligence*, PP, 08 2019. doi: 10.1109/TPAMI.2019.2935715.
- A. Borji, H. Rezazadegan Tavakoli, D. Sihite, and L. Itti. Analysis of scores, datasets, and models in visual saliency prediction. pages 921–928, 12 2013. doi: 10.1109/ICCV.2013.118.
- M. Brill. *Trichromatic Theory*, pages 827–829. 01 2014. ISBN 978-0-387-30771-8.
- N. Bruce and J. Tsotsos. Saliency based on information maximization. volume 18, 01 2005.
- M. Butz. Toward a cognitive sequence learner: Hierarchy, self-organization, and top-down bottom-up interaction. 04 2004.
- Z. Bylinskii, T. Judd, A. Oliva, A. Torralba, and F. Durand. What do different evaluation metrics tell us about saliency models? *arXiv preprint arXiv:1604.03605*, 2016.
- M. Cornia, L. Baraldi, G. Serra, and R. Cucchiara. A deep multi-level network for saliency prediction. 09 2016. doi: 10.1109/ICPR.2016.7900174.
- M. Emami and L. Hoberock. Selection of a best metric and evaluation of bottom-up visual saliency models. *Image and Vision Computing*, 31:796–808, 10 2013. doi: 10.1016/j.imavis.2013.08.004.
- U. Engelke, H. Liu, J. Wang, P. Le Callet, I. Heynderickx, H.-J. Zepernick, and A. Maeder. A comparative study of fixation density maps. *IEEE transactions on image processing : a publication of the IEEE Signal Processing Society*, 11 2012. doi: 10.1109/TIP.2012.2227767.
- M. Feng. Evaluation toolbox for salient object detection. https://github.com/ArcherFMY/sal_eval_toolbox, 2018.

- G. Finlayson, M. Drew, and B. Funt. Color constancy: Enhancing von kries adaptation via sensor transformations. *Proc SPIE*, 1913, 09 1993. doi: 10.1117/12.152721.
- G. Finlayson, A. Alsam, and S. Hordley. Local linear models for improved von kries adaptation. pages 139–144, 01 2002.
- S. Goferman, L. Zelnik-Manor, and A. Tal. Context-aware saliency detection. pages 2376 – 2383, 07 2010. doi: 10.1109/CVPR.2010.5539929.
- C. Guo, Q. Ma, and L. Zhang. Spatio-temporal saliency detection using phase spectrum of quaternion fourier transform. 06 2008. doi: 10.1109/CVPR.2008.4587715.
- A. Haar. Zur theorie der orthogonalen funktionensysteme. (zweite mitteilung). *Mathematische Annalen*, 71:38–53, 1912. URL <http://eudml.org/doc/158516>.
- J. Harel. A saliency implementation in matlab. <http://www.klab.caltech.edu/~harel/share/gbvs.php>, 2012.
- X. Hou and L. Zhang. Saliency detection: A spectral residual approach. volume 2007, 06 2007. doi: 10.1109/CVPR.2007.383267.
- X. Hou and L. Zhang. Dynamic visual attention: Searching for coding length increments. volume 21, pages 681–688, 01 2008.
- X. Hou, J. Harel, and C. Koch. Image signature: Highlighting sparse salient regions. *IEEE transactions on pattern analysis and machine intelligence*, 34, 07 2011. doi: 10.1109/TPAMI.2011.146.
- L. Hurvich and D. Jameson. An opponent-process theory of color vision. *Psychological Review*, 64:384–404, 12 1957. doi: 10.1037/h0041403.
- N. imamoğlu, W. Lin, and Y. Fang. A saliency detection model using low-level features based on wavelet transform. *IEEE Transactions on Multimedia*, 15:96–105, 01 2013. doi: 10.1109/TMM.2012.2225034.
- L. Itti. Models of bottom-up and top-down visual attention. 01 2000.
- L. Itti, C. Koch, and E. Niebur. A model of saliency-based visual attention for rapid scene analysis. *Pattern Analysis and Machine Intelligence, IEEE Transactions on*, 20:1254 – 1259, 12 1998. doi: 10.1109/34.730558.
- T. Jost, N. Ouerhani, R. Wartburg, R. Müri, and H. Hügli. Assessing the contribution of color in visual attention. *comput. vis. image und.* 100, 107-123. *Computer Vision and Image Understanding*, 100:107–123, 10 2005. doi: 10.1016/j.cviu.2004.10.009.
- T. Judd, F. Durand, and A. Torralba. A benchmark of computational models of saliency to predict human fixations. In *MIT Technical Report*, 2012.
- J. Krauskopf and K. Gegenfurtner. Color discrimination and adaptation. *Vision research*, 32:2165–75, 12 1992. doi: 10.1016/0042-6989(92)90077-V.
- S. Kruthiventi, V. Gudisa, J. Dholakiya, and R. Babu. Saliency unified: A deep architecture for simultaneous eye fixation prediction and salient object segmentation. pages 5781–5790, 06 2016. doi: 10.1109/CVPR.2016.623.
- M. Kümmerer, T. Wallis, and M. Bethge. Information-theoretic model comparison unifies saliency metrics. *Proceedings of the National Academy of Sciences*, 112:201510393, 12 2015a. doi: 10.1073/pnas.1510393112.
- M. Kümmerer, T. Wallis, and M. Bethge. Information-theoretic model comparison unifies saliency metrics. *Proceedings of the National Academy of Sciences*, 112:201510393, 12 2015b. doi: 10.1073/pnas.1510393112.
- M. Kümmerer, T. Wallis, and M. Bethge. Deepgaze ii: Reading fixations from deep features trained on object recognition. 10 2016.
- J. li, M. Levine, X. An, X. Xu, and H. He. Visual saliency based on scale-space analysis in the frequency domain. *IEEE Transactions on Pattern Analysis and Machine Intelligence*, 35:996–1010, 11 2012. doi: 10.1109/TPAMI.2012.147.
- A. Louis, P. Maass, and A. Rieder. *Wavelets: Theory and Applications*. 01 1997. ISBN 978-0-471-96792-7.
- J. Mannos and D. Sakrison. The effects of a visual fidelity criterion of the encoding of images. *IEEE Transactions on Information Theory*, 20(4):525–536, 1974.
- D. Mercy. A review of automatic gain control theory. *Radio and Electronic Engineer*, 51, 01 1981. doi: 10.1049/ree.1981.0084.
- K. Mullen. The contrast sensitivity of human color vision to red-green and blue-yellow chromatic gratings. *The Journal of physiology*, 359:381–400, 03 1985. doi: 10.1113/jphysiol.1985.sp015591.
- N. Murray, M. Vanrell, X. Otazu, and C. A. Párraga. Saliency estimation using a non-parametric low-level vision model. pages 433–440, 06 2011. doi: 10.1109/CVPR.2011.5995506.

- N. Murray, M. Vanrell, X. Otazu, and C. A. Párraga. Low-level spatiochromatic grouping for saliency estimation. *IEEE transactions on pattern analysis and machine intelligence*, 35:2810–6, 11 2013. doi: 10.1109/TPAMI.2013.108.
- N. Riche, M. Mancas, B. Gosselin, and T. Dutoit. Rare: A new bottom-up saliency model. 10 2012. doi: 10.1109/ICIP.2012.6466941.
- N. Riche, M. Duvinage, M. Mancas, B. Gosselin, and T. Dutoit. Saliency and human fixations: State-of-the-art and study of comparison metrics. 12 2013. doi: 10.1109/ICCV.2013.147.
- B. Schauerte and R. Stiefelhagen. Quaternion-based spectral saliency detection for eye fixation prediction. pages 116–129, 10 2012. ISBN 978-3-642-33708-6. doi: 10.1007/978-3-642-33709-3\9.
- A. Selvaraj and N. Shebiah. Object recognition using wavelet based salient points. *The Open Signal Processing Journal*, 2:14–20, 09 2009. doi: 10.2174/1876825300902010014.
- H. Seo and P. Milanfar. Static and space-time visual saliency detection by self-resemblance. *Journal of vision*, 9: 15.1–27, 11 2009. doi: 10.1167/9.12.15.
- R. Shapley and M. Hawken. Color in the cortex: Single- and double-opponent cells. *Vision research*, 51:701–17, 02 2011. doi: 10.1016/j.visres.2011.02.012.
- M. Spratling. Predictive coding as a model of the v1 saliency map hypothesis. *Neural networks : the official journal of the International Neural Network Society*, 26:7–28, 10 2011. doi: 10.1016/j.neunet.2011.10.002.
- Y. Sun and R. Fisher. Object-based visual attention for computer vision. *Artificial Intelligence*, 146:77–123, 05 2003.
- A. Treisman and G. Gelade. A feature-integration theory of attention. *Cognitive psychology*, 12:97–136, 02 1980.
- D. Wang, A. Kristjansson, and K. Nakayama. Efficient visual search without top-down or bottom-up guidance. *Perception & psychophysics*, 67:239–53, 03 2005. doi: 10.3758/BF03206488.
- A. Watson and A. Ahumada. The spatial standard observer. *Journal of Vision - J VISION*, 4:51–51, 01 2010. doi: 10.1167/4.8.51.
- A. Watson and J. Malo. Video quality measures based on the standard spatial observer. volume 3, pages III–41, 02 2002. ISBN 0-7803-7622-6. doi: 10.1109/ICIP.2002.1038898.
- N. Wilming, T. Betz, T. Kietzmann, and P. König. Measures and limits of models of fixation selection. *PloS one*, 6: e24038, 09 2011. doi: 10.1371/journal.pone.0024038.
- J. Zhang and S. Sclaroff. Saliency detection: A boolean map approach. pages 153–160, 12 2013. doi: 10.1109/ICCV.2013.26.
- L. Zhang, M. Tong, T. Marks, H. Shan, and G. Cottrell. Sun: A bayesian framework for saliency using nature statistics. *Journal of vision*, 8:32.1–20, 02 2008. doi: 10.1167/8.7.32.
- L. Zhaoping. A neural model of contour integration in the primary visual cortex. *Neural computation*, 10:903–40, 05 1998. doi: 10.1162/089976698300017557.